Conductivity of multiwall carbon nanotubes: Role of multiple shells and defects

A. Stetter, J. Vancea, and C. H. Back
Universität Regensburg, Universitätsstraße 31, 93040 Regensburg, Germany
(Received 4 June 2010; revised manuscript received 26 July 2010; published 29 September 2010)

We report on laterally resolved measurements of the current-induced gradient in the electrochemical potential of multiwall carbon nanotubes. Nanotubes with different classes of defects were studied at room temperature. The potential profile of the outermost shell along the tube was measured in a local as well as in a nonlocal geometry. The data have been used to separate the contributions of various shells to the total resistance of the whole tube. For this purpose, a classical resistivity model was used that describes the measured potential profiles well. Additionally, the influence of structural defects on the conductivity has been quantified. Particularly, defects such as an ending outermost shell, an intratube junction, and a plastically stretched tube with a kink were investigated.

DOI: 10.1103/PhysRevB.82.115451 PACS number(s): 73.63.Fg

Although multiwall carbon nanotubes (MWCNTs) were apparently first imaged in the 1950s,[1] modern nanotube research was triggered by Iijima in 1991.[2] In his experiments, the spatial resolution was good enough to reveal their multiple shell configuration. Soon conductivity measurements were carried out to determine the electronic properties of MWCNTs. Several studies on free standing or suspended tubes report ballistic as well as diffusive electron transport at room temperature.[3–6]

Since typically only the outermost shell is contacted the contribution of inner shells to the conductivity is directly connected with the intershell conductivity. Several groups reported that the current flows predominantly in the outermost shell.[3,7] Calculations, however, are discordant.[8–13] They predict suppressed intershell transport for a long tube[10] but also that the electronic wave function may spread over several shells.[9] Measurements on tubes with removed outer shells between the contacts and telescopically extended tubes revealed that the intershell conductivity cannot be neglected.[14,15] Bourlon *et al.*[16] determined the intershell conductivity with local and nonlocal four-point measurements using an array of evaporated contact electrodes. They report a value of the intershell conductance per length of $\approx(10\ \mathrm{k}\Omega)^{-1}/\mu\mathrm{m}$. Using scanning probe potentiometry techniques with less invasive voltage probes, we reported in a previous paper that the intershell conductivity can exceed this value by more than one order of magnitude.[17]

In this paper, we expand the resistivity model proposed by Bourlon *et al.*[16] and solve it for various MWCNT configurations. In particular, we compare our experimental results obtained on MWCNTs with different types of defects with the results obtained from the simulations. Our results show that the extracted values of the shell resistivities as well as the intershell conductivity may depend on the type of contacts used in the experiment.

In Ref. 17, we used a numerical simulation based on the resistivity model proposed by Bourlon *et al.*[16] with current injection at a single point. Here we improve this model by introducing spatially extended current driving electrodes. In the diffusive limit, the voltage $V_i(x)$ and current $I_i(x)$ for shell i are linked to the intrashell resistivity ρ_i by

$$\frac{dV_i(x)}{dx} = -\rho_i I_i(x). \tag{1}$$

The variation of $I_i(x)$ is given by the intershell current between shell i and neighboring shells. For the outermost shell below, one electrode one obtains, for example,

$$\frac{dI_1(x)}{dx} = -g[V_1(x) - V_2(x)] - \sigma[V_1(x) - V_0] \tag{2}$$

with g being the intershell conductivity between outermost and second shell and σ the contact conductivity to the electrode with the constant voltage V_0 ($\rho_0=0$ if the metal electrode is highly conductive). Forming individual differential equation systems for the regions below, between and beyond the electrodes and connecting them with boundary conditions results in an extensive but analytically solvable equation system. The boundary conditions result from the continuity equation for the current and take the discontinuity of the electrodes into account. Due to limited computing power solving the model is reasonable only for symmetrical configurations with two shells. Despite these simplifications, the model gives a fairly good picture of the underlying physics. For a MWCNT contacted by two electrodes, the model predicts a slightly bent potential profile with higher slope near the electrodes and an exponential-like behavior beyond the electrodes. The latter is a pure exponential decrease for infinitely long tubes but is slightly distorted in other cases, see fit in Fig. 2(a).

Our experimental setup and the measurement technique was reported before and is illustrated in Fig. 1.[17] Tubes are contacted by two metal electrodes. We drive a constant current through the electrodes (typically $I_s=1\ \mu\mathrm{A}$) and measure the local potential using a scanning tunneling microscope (STM) tip and by recording I-V curves at each point along the tube with the feedback control switched off.

For reference reasons first a MWCNT with $d\approx 33$ nm and no obvious defects (sample A) was contacted with metal electrodes. The contacts are evaporated asymmetrically to have a sufficiently long part of the tube beyond the contacts in order to allow local as well as nonlocal measurements. The whole potential profile recorded at room temperature of

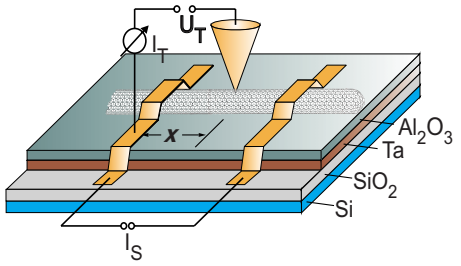

FIG. 1. (Color online) The potentiometric setup. MWCNTs are deposited on the $Al_2O_3/Ta/SiO_2/Si$ surfaces and contacted with two Pd/Au contacts using electron-beam lithography and standard lift off techniques. A fixed constant current of typically $I_s=1$ μA is sent through the tube and local *I-V* characteristics are measured using a STM tip.

local and nonlocal measurements is shown in Fig. 2(a) (black filled circles) for a current of $I_s=1$ μA. The bending of the local potential is noticeable as well as a decrease in the nonlocal potential, both predicted by the present resistivity model.

The best-fit [solid red line in Fig. 2(a)] results in the following set of parameters:

resistivity of outer shell:

$$\rho_1 = 52 \pm 5 \ \text{k}\Omega/\mu\text{m},$$

resistivity of second shell:

$$\rho_2 = 9 \pm 3 \ \text{k}\Omega/\mu\text{m},$$

intershell conductivity:

$$g = (220 \ \Omega)^{-1} 1/\mu\text{m} \pm 7 \times 10^{-4} \ \Omega^{-1}/\mu\text{m},$$

contact conductivity:

$$\sigma = (150 \ \Omega)^{-1} 1/\mu\text{m} \pm 2 \times 10^{-5} \ \Omega^{-1}/\mu\text{m}.$$

The value of ρ_2 is mainly extracted from the bending of the potential between the electrodes and therefore has a relatively high error of about 30%. The value of ρ_1 is directly connected with the potential profile of the outermost shell and can therefore be extracted more precisely. The current that exits the part of the tube between the electrodes depends strongly on g and can be extracted mainly from the potential step between the electrode and the nonlocal potential at about −250 nm. The contact conductivity σ, however, shifts the potential jumps at both sides of the electrode ($x=0$ nm, $x=-240$ nm) and can be determined very exactly.

The difference between ρ_1 and ρ_2 is remarkably high and far beyond the error bars. Bourlon *et al.*[16] interpreted these differences with the existence of adsorbents or defects in the outermost shell whereas the lower shells are protected by the outermost one. Another interpretation is that the outermost shell has a chiral vector of a semiconducting shell and the inner tube is metallic.

The deviation for $x>400$ nm can easily be explained by the asymmetry of the contact electrodes. To significantly reduce the computing time, the fit has been performed with a symmetric configuration, with the tube protruding from both contacts. Thus, the configuration of the right part of the tube ending directly below the contact cannot be reproduced exactly. In fact, for shorter tubes the model predicts a stronger bending and a higher slope [Fig. 2(b)] as observed experimentally. Additionally the current distribution [Fig. 2(c)] shows that our model reproduces the results of Nemec *et al.*[18] which show that current injection for highly transparent contacts occurs predominantly at the edges of the electrodes.

The second tube studied (sample B) in our experiments shows a diameter change at $x=270$ nm from $d\approx 24$ nm to $d\approx 29$ nm probably due to an intramolecular junction.[19] The potential profile [Fig. 3(a)] exhibits two distinct regions corresponding to the two sectors of different diameters. For the sector connecting to the right contact, local as well nonlocal measurements could be done. These measurements can also be fitted well using our resistivity model (red line in Fig. 3). The fit parameters are

$$\rho_1 = 47 \pm 5 \ \text{k}\Omega/\mu\text{m},$$

$$\rho_2 = 40 \pm 8 \ \text{k}\Omega/\mu\text{m},$$

$$g = (1 \ \text{k}\Omega)^{-1} 1/\mu\text{m} \pm 2 \times 10^{-4} \ \Omega^{-1}/\mu\text{m},$$

$$\sigma = (200 \ \Omega)^{-1} 1/\mu\text{m} \pm 5 \times 10^{-5} \ \Omega^{-1}/\mu\text{m}.$$

For the sector connecting to the right contact, no nonlocal potential measurements could be performed due to the fluc-

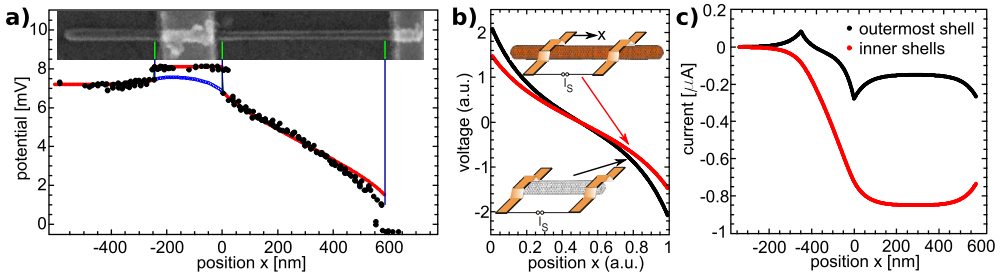

FIG. 2. (Color online) (a) Potential profile of sample A (black dots). For $-240<x<0$ nm and $x>590$ nm, the measurements were performed on the contact electrodes [see scanning electron microscopy (SEM) image in upper inset]. The calculated potential profile (solid red curve and blue circles below the contact) agrees well with the measurements, in particular, for $x<400$ nm. (b) Influence of the protruding part of the tube in the model [black: hypothetic tube only between the contacts (schematics: lower inset); red: long tube where a symmetric protruding part was added (schematics: upper inset)]. (c) Calculated current distribution.

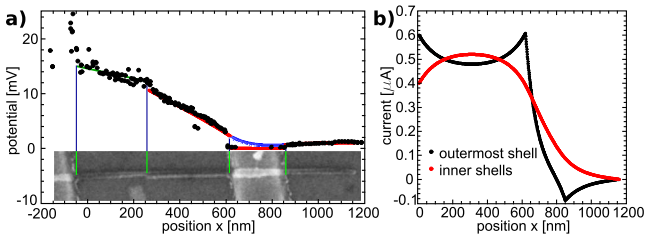

FIG. 3. (Color online) (a) Measured potential profile of sample B. The contact resistance of the left electrode was fluctuating resulting in an unstable potential for $x<0$. The green line illustrates the mean slope of the potential of the left sector of the tube. The red line (blue below the contact) is the fit to the resistivity model. Inset: SEM image of sample B with electrodes. (b) Calculated current distribution.

tuating contact resistivity. Therefore and due to the bad signal to noise ratio for $x<270$ nm, a reasonable fit for the left part of the tube was not possible. For a rough estimate of the main differences, we can use the mean gradient (green line in Fig. 3) that is much lower than for the thicker sector corresponding to a mean resistivity of 10 $k\Omega/\mu m$ compared to a mean resistivity of 24 $k\Omega/\mu m$ of the right sector. Assuming a similar defect density in the crystal lattice in both sectors, we conclude that at least one of the shells must have a transition from a metallic to a semiconducting tube. The anomaly at the defect position can be due to a Schottky barrier.

Sample C, originally "defectless," was stretched and kinked by applying a force perpendicular to the tube axis with the STM tip (see lower inset of Fig. 4). In this procedure, the two point resistivity between the contacts increased irreversibly from 21 to 49 $k\Omega$ indicating plastic deformations in the tube.[20,21] The deformation of the left electrode (upper inset of Fig. 4) indicates that the tube moved with respect to the contact during stressing.[22] The originally uniform diameter of ≈ 19 nm is decreased for parts II and III which are separated by the 90° kink. Comparing the total length of the tube before and after manipulation, we find an elongation of 130 nm which can be attributed to sectors II and III only. The corresponding strain in these regions is 20%. Elongations of this magnitude were already observed

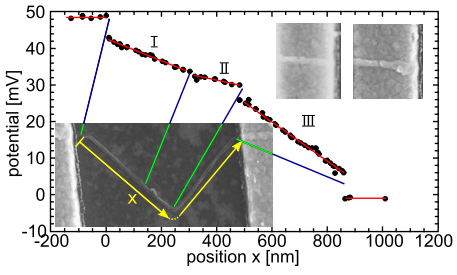

FIG. 4. (Color online) Sample C exhibits three regions with different electronic properties corresponding to the modifications of the tube. At $x=300$ nm, the tube is narrowed from a diameter $d\approx 19$ nm to $d\approx 14$ nm. The kink at $x=480$ nm causes a strong increase in the slope of the potential profile. The resistivities are 30 $k\Omega/\mu m$, 15 $k\Omega/\mu m$, and 53 $k\Omega/\mu m$ for parts I, II, and III, respectively. The upper inset compares the left electrode before (left) and after (right) manipulation.

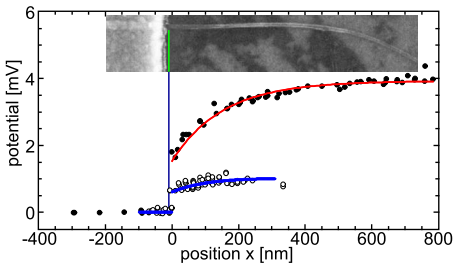

FIG. 5. (Color online) Nonlocal potential profile of sample C (black filled dots) compared to the nonlocal voltage of sample A (open dots), each with the according fit. In case of sample C, the tube is long enough ($\gg L_a$) that it behaves purely exponentially (red line) as predicted by the model for long tubes.

for single-wall nanotubes[20] and theoretically described as formation of (5-7-7-5) defects with followed plastic flow (ductile behavior).[23]

The locally measured potential profile (Fig. 4) exhibits three different slopes corresponding to the V structure. The resistivity does not scale directly with the diameter. Parts II and III have similar diameters but exhibit strongly differing slope values. The kink separating part II and III induces a potential step indicating a tunnel barrier.[24] Although part II is narrowed and therefore obviously defective its resistivity is closer to the expected value before manipulation. The other parts have a highly increased resistivity. The potential steps at the edges of the contacts are now larger than for previous samples. This is a result of the increased tube resistivity at the border area below the contact that shifts the injection zone to the middle of the contact. Therefore the resistance increase is mainly connected to a change in the intrinsic tube resistivity. The left contact resistance where the tube was pulled out has not changed as dramatically as reported by Paulson *et al.*[22]

The part of the tube outside of the contacts is not altered during manipulation and therefore should exhibit original properties. Nevertheless the modification between the contacts influences the nonlocal potential since it defines how the current spreads over the shells. A large defect density increases scattering events and therefore the probability of scattering into a neighboring shell. It was also shown that broken bonds can rearrange with other shells increasing the intershell conductivity.[25] Consequently, it is not completely surprising that the nonlocal potential is larger than that of the previous samples, indicating a larger amount of current flowing in the inner shells (Fig. 5). The decay length $L_a=(\sqrt{g(\rho_1+\rho_2)})^{-1}$, however, is an intrinsic property of the protruding part of the tube. The exponential fit determines $L_a=154$ nm which is in the same range as that of sample B ($L_a=110$ nm).

All our results are based on a model including only two complete shells. Considering the current distribution, e.g., of sample A [Fig. 2(c)] we realize that the inner shell carries more than 80% of the total current. Thus the assumption that only the two outermost shells are relevant for transport has to be reconsidered. In fact ρ_2 can be viewed as an effective resistivity of an inner tube consisting of the second shell and the shells below. This approximation is plausible because

even for configurations with strongly different resistivities of the shells (like in sample A) the resulting potential profile is roughly linear, i.e., tolerates a uniform resistivity.

The deduced intrashell resistivities are slightly larger than the results of Bourlon *et al.*[16] On the other hand, our intershell conductances are up to a factor of 100 higher. To explain these differences, we try to argue with two different reasons. First, the tubes investigated in our work are thicker by a factor of approximately 2. Including the differences in the tube diameter and therefore also a factor of 2 in the perimeter and the contact area reduces the discrepancies but leaves a deviation in the intershell conductance of more than one order of magnitude. For diameters larger than 15–20 nm, polygonal cross sections have been observed.[26,27] In this range, the intershell spacings of about 0.39 nm for small diameters decrease to nearly that of graphite of 0.34 nm.[28] The results above mentioned indicate that for large diameters the tubes consist of several planar regions joined together. It was suggested that in these planar regions the stacking is closely commensurate to the graphitic stacking. In such tube sectors, it is obvious that the intershell coupling should approach that of graphite. Including the tube perimeter and the intershell distance, we obtain an intershell resistivity which is larger than that of graphite by three orders of magnitude.[29] Consequently, we can exclude complete graphitic stacking even for small sides of the polygonal cylinder. In fact, if planar regions in our tubes exist the interlayer coupling is strongly decreased probably due to incommensurate stacking. This reduction in the interlayer coupling was also observed in twisted graphene.[30]

Furthermore, for thicker tubes the one-dimensional subbands are moving together giving rise to the suspicion that the unavoidable doping causes more channels contributing to electron transport. Our measurement, however, reveals higher values for the intrashell resistivities. Consequently, the difference in diameter alone cannot be responsible for the discrepancy between the experimental data.

The second argument can be provided by the differences in the electrical contacting of the tubes. Bourlon *et al.*[16] evaporated several fixed contacts with a width of 200 nm separated by a 200 nm metal-free tube. Therefore about one half of the tube was coated with metal. With the model presented here, we calculated a configuration with an additional electrode in the middle of the tube which does not inject

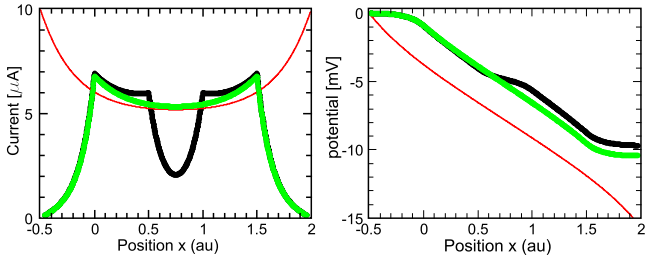

FIG. 6. (Color online) Comparison between a configuration with only two contacting electrodes ($x<0$ and $x>1.5$) (green line) and with an additional electrode in the middle ($0.5<x<1$) (black line). The result of the model with current injection at a single point (Ref. 16) is also shown (thin red line).

electric current (Fig. 6). This single additional electrode modifies the current distribution significantly. The current exits the tube at the beginning of the middle contact and reenters the tube again at the other border resulting in a reduced effective resistivity. Since this electrode carries a part of the current, the current in the inner shell is also reduced. Consequently, the current is more localized in the outermost shell between the electrodes. Additional contacts increase this effect. In fact the different contacting setups explain the discrepancies: the resistivity is reduced by additional contacts and at the same time the current flows preferentially in the outermost shell giving a reduced intershell conductance.

In conclusion, we reported on laterally resolved local and nonlocal potential profiles of MWCNTs without and with obvious defects during current flow. The potential decreases continuously indicating diffusive transport. From these profiles, we separated the contributions of outer and inner shells and determined the intershell conductivity by fitting with a resistivity model. The differences between our results and previously reported ones could be traced back to a lower interference of our voltage probe with the tube. Furthermore, the influence of specific defects in the tube structure on transport behavior was determined. Particularly, changes in the tube conductivity or steps in the potential profile could be directly assigned to specific structural defects.

We gratefully acknowledge fruitful discussions with C. Strunk and financial support from the DFG via SFB 689.

[1] L. V. Radushkevich and V. M. Lukyanovich, Zurn. Fisic. Chim. **26**, 88 (1952).
[2] S. Iijima, Nature (London) **354**, 56 (1991).
[3] S. Frank, P. Poncharal, Z. L. Wang, and W. A. de Heer, Science **280**, 1744 (1998).
[4] A. Urbina, I. Echeverría, A. Pérez-Garrido, A. Díaz-Sánchez, and J. Abellán, Phys. Rev. Lett. **90**, 106603 (2003).
[5] A. Bachtold, M. S. Fuhrer, S. Plyasunov, M. Forero, E. H. Anderson, A. Zettl, and P. L. McEuen, Phys. Rev. Lett. **84**, 6082 (2000).
[6] K. Liu, P. Avouris, R. Martel, and W. K. Hsu, Phys. Rev. B **63**, 161404 (2001).
[7] A. Bachtold, C. Strunk, J.-P. Salvetat, J.-M. Bonard, L. Forró, T. Nussbaumer, and C. Schönenberger, Nature (London) **397**, 673 (1999).
[8] S. Sanvito, Y.-K. Kwon, D. Tománek, and C. J. Lambert, Phys. Rev. Lett. **84**, 1974 (2000).
[9] S. Roche, F. Triozon, A. Rubio, and D. Mayou, Phys. Rev. B **64**, 121401 (2001).
[10] Y.-G. Yoon, P. Delaney, and S. G. Louie, Phys. Rev. B **66**, 073407 (2002).
[11] A. Hansson and S. Stafström, Phys. Rev. B **67**, 075406 (2003).

[12] F. Triozon, S. Roche, A. Rubio, and D. Mayou, Phys. Rev. B **69**, 121410 (2004).
[13] A. M. Lunde, K. Flensberg, and A. P. Jauho, Phys. Rev. B **71**, 125408 (2005).
[14] P. G. Collins, M. S. Arnold, and P. Avouris, Science **292**, 706 (2001).
[15] J. Cumings and A. Zettl, Phys. Rev. Lett. **93**, 086801 (2004).
[16] B. Bourlon, C. Miko, L. Forró, D. C. Glattli, and A. Bachtold, Phys. Rev. Lett. **93**, 176806 (2004).
[17] A. Stetter, J. Vancea, and C. H. Back, Appl. Phys. Lett. **93**, 172103 (2008).
[18] N. Nemec, D. Tománek, and G. Cuniberti, Phys. Rev. Lett. **96**, 076802 (2006).
[19] Z. Yao, H. W. Ch. Postma, L. Balents, and C. Dekker, Nature (London) **402**, 273 (1999).
[20] D. Bozovic, M. Bockrath, J. H. Hafner, C. M. Lieber, H. Park, and M. Tinkham, Phys. Rev. B **67**, 033407 (2003).
[21] T. Kuzumaki and Y. Mitsuda, Appl. Phys. Lett. **85**, 1250 (2004).
[22] S. Paulson, M. R. Falvo, N. Snider, A. Helser, T. Hudson, A. Seeger, R. M. Taylor, R. Superfine, and S. Washburn, Appl. Phys. Lett. **75**, 2936 (1999).
[23] M. Buongiorno Nardelli, B. I. Yakobson, and J. Bernholc, Phys. Rev. Lett. **81**, 4656 (1998).
[24] M. J. Biercuk, N. Mason, J. M. Chow, and C. M. Marcus, Nano Lett. **4**, 2499 (2004).
[25] S. Agrawal, M. S. Raghuveer, H. Li, and G. Ramanath, Appl. Phys. Lett. **90**, 193104 (2007).
[26] M. Liu and J. M. Cowley, Ultramicroscopy **53**, 333 (1994).
[27] J. M. Cowley and S. D. Packard, Ultramicroscopy **63**, 39 (1996).
[28] C. H. Kiang, M. Endo, P. M. Ajayan, G. Dresselhaus, and M. S. Dresselhaus, Phys. Rev. Lett. **81**, 1869 (1998).
[29] K. Matsubara, K. Sugihara, and T. Tsuzuku, Phys. Rev. B **41**, 969 (1990).
[30] H. Schmidt, T. Lüdtke, P. Barthold, and R. J. Haug, Phys. Rev. B **81**, 121403 (2010).